Journal of Polymer Science

WILEY

JOURNAL OF POLYMER SCIENCE

RESEARCH ARTICLE OPEN ACCESS

Thermal and Mechanical Properties of Lignin Derivative–Sulfur Composites

Nawoda L. Kapuge Dona | Perla Y. Sauceda-Oloño | Rhett C. Smith

Department of Chemistry, Clemson University, Clemson, South Carolina, USA

Correspondence: Rhett C. Smith (rhett@clemson.edu)

Received: 5 July 2024 | **Revised:** 30 October 2024 | **Accepted:** 31 October 2024

Funding: This work was supported by the National Science Foundation, CHE-2203669.

Keywords: guaiacol | lignin | sulfur | sustainable composites | syringol

ABSTRACT

Lignin, comprising 20%–35% of lignocellulosic biomass, is the second most abundant biopolymer after cellulose. As the bioethanol industry expands, the accumulation of lignin by-products necessitates innovative valorization strategies. This study explores the synthesis and characterization of lignin-derived composites. Specifically, the reaction of 20 wt. % lignin-derived guaiacol or syringol with 80 wt. % elemental sulfur gives composites GS_{80} and SS_{80}, respectively. The chemical structures of composites were elucidated using GC–MS, ^{1}H NMR, and UV–Vis spectroscopy, revealing the formation of both S—C_{aryl} and S—C_{alkyl} bonds. Thermal and morphological analysis (via TGA, DSC, PXRD, and SEM-EDS) indicated SS_{80} has higher crystallinity and thermal stability than GS_{80}, attributed to a higher degree of crosslinking and a greater content of dark sulfur. Mechanical testing showed SS_{80} exhibits superior compressional and flexural strengths, and enhanced Young's modulus and Shore hardness, compared to GS_{80}. Notably, the mechanical strength parameters for SS_{80} are comparable to those of C62 class bricks used in construction applications. These findings suggest that lignin-derived composites, particularly those incorporating syringol, can provide viable alternatives to traditional materials in various applications, contributing to both waste valorization and sustainable materials science.

1 | Introduction

Lignin constitutes approximately 20%–35% of lignocellulosic biomass, making it the second most abundant natural polymer after cellulose [1–4]. As the extraction of cellulose from lignocellulosic biomass intensifies to support the growing green ethanol economy [5, 6], a concomitant increase in lignin by-product is inevitable. This burgeoning accumulation of lignin poses a significant disposal challenge but presents an opportunity for valorization into valuable chemicals and materials. Among the various valorization strategies, the thermal decomposition (thermolysis) [7–10] or chemical decomposition (solvolysis) [11–14] of lignin offers a pathway to small aromatic molecules such as guaiacol, syringol, vanillin, ferulic acid, eugenol, creosol, and sinapyl alcohol derivatives [12, 15–18]. Such lignin derivatives have been functionalized to give monomers for polyacetals, polyesters, polycarbonates, polyacrylics, epoxy resins, and polyurethanes exhibiting diverse properties [19–23]. Lignin-derived bisguaiacols, for example, hold promise as bio-based alternatives for non-isocyanate polyurethane thermosets, offering significantly improved toughness and elongation at break compared to bisphenol-based benchmarks [24, 25]. Syringaldehyde has been used to fabricate supramolecular plastic with high tensile strength, water stability, biodegradability, recyclability, UV resistance, and antibacterial properties [26]. Bio oils, mixtures of small molecular lignin-derived compounds, have also been successfully utilized for high-performance additive [27, 28]. These are only a few of the more recent efforts to harness lignin-derived aromatics in polymer synthesis.

Another industrial problem is the disposal of sulfur. Sulfur is a by-product generated at 80 MT excess per year during fossil fuel

refining processes [29–31]. Surplus sulfur utilization demands innovative approaches for its repurposing to align with sustainability goals. Reactions of sulfur with phenol derivatives like bisphenol A [32–34], biomass derivatives [35–38], fats/oils [39–48], and terpenes [49–51] have yielded a range of high sulfur-content materials (HSMs) with applications ranging from plastic optical components [52–56] and Li-S battery materials [35, 57–66] to fertilizers [67–69], water remediation absorbents [41, 70–82], adhesives [39, 83, 84], and structural materials [37, 85–97].

Several studies have been undertaken concerning combining lignin-derived aromatics with elemental sulfur [36, 37, 86, 98–104]. An especially pertinent study by Karunarathna et al. illustrated that guaiacol reacts with elemental sulfur to form novel composites designated as GS_x (where *x* indicates the wt. % elemental sulfur in the monomer feed). Spectroscopic and GC–MS studies on the polymer and depolymerization fragments thereof revealed that a complex set of mechanistic pathways contribute to the microstructure of GS_x including S—C_{aryl} bond formation and methoxy-to-hydroxyl conversion via C—O sigma bond scission (Scheme 1). Composites GS_{80} exhibited promising mechanical properties surpassing those of many other HSMs. However, the investigation of GS_x composites primarily focused on tensile properties, leaving a gap in knowledge regarding their flexural and compressional strengths and morphological properties.

Inspired by recent studies on HSMs, we hypothesized that composites could be synthesized utilizing syringol, a major component of many lignins [1, 12], as a starting material. Consequently, this paper reports on our exploration into forming a new composite, SS_{80}, prepared by the reaction of 80 wt. % elemental sulfur with 20 wt. % syringol. This study elucidates mechanistic insight into bond-forming and bond-breaking reactions contributing to the molecular structure of SS_{80}. We extend our investigation to compare the thermal, morphological, and mechanical strength properties of SS_{80} against those of GS_{80}, other HSMs, and commercial building materials that may be replaceable by more sustainably sourced materials like GS_{80} or SS_{80}.

2 | Results and Discussion

2.1 | Design, Synthesis, and Chemical Characterization

Karunarathna et al. reported that the reaction of guaiacol (10–20 wt. %) and elemental sulfur (80–90 wt. %) at 230°C leads to the formation of composites GS_x (x = wt. % sulfur in the monomer feed) [98]. Under these conditions, a complex set of reaction pathways were observed, including S—C_{aryl} bond formation, C—O σ-bond scission, –OCH_3 methyl migration, S—$C_{benzylic}$ bond formation involving the migrated methyl group, and even dearomatization reactions leading to quinone derivatives that participated in subsequent S—C_{alkyl} bond formation (Scheme 1). These mechanisms were found to be highly conserved in recently reported small molecule studies on reactions of elemental sulfur with a range of lignin derivatives [100, 104, 105].

The previous report on GS_x composites left several questions unaddressed, among which were (1) to what extent does changing the substituents on the aryl ring influence chemical microstructures of composites, (2) how do differences in reactivity and substitution pattern influence morphology, thermal, and mechanical properties, and (3) what are the flexural and compressional strengths of the composites (not reported in prior work on GS_x). The current work addresses these questions by synthesizing a sulfur–syringol composite and assessing a more complete set of mechanical parameters for both GS_{80} and SS_{80}.

Following the procedure for preparing GS_{80}, syringol (20 wt. %) and sulfur (80 wt. %) were heated under nitrogen in a sealed pressure vessel to 230°C tube for 24 h to give composite SS_{80}.

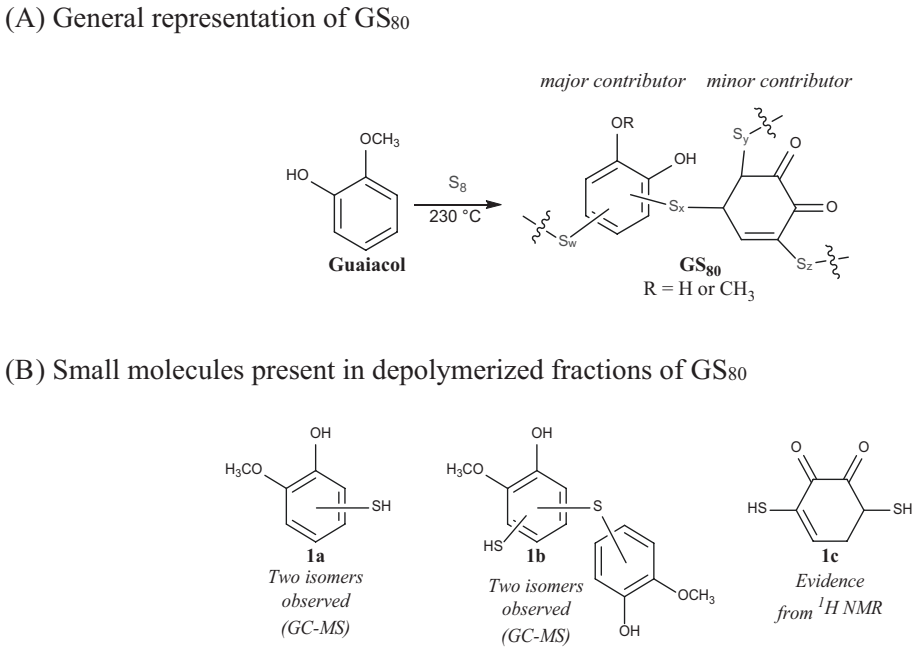

SCHEME 1 | The reaction of guaiacol and elemental sulfur leads to composite GS_{80} (A), an assignment assisted by analysis of depolymerization fragments (B) and spectroscopic data.

After cooling to room temperature, SS_{80} is a remeltable dark brown solid. SS_{80} can thus be easily shaped by pouring the molten composite into a silicone mold and allowing the material to cool, a method used to create samples appropriate for tensile, flexural, and compressional strength tests (Figure 1).

Given the range of mechanistic pathways reported for reactions of sulfur with anisole derivatives (i.e., Scheme 1), it was of interest to determine the extent to which these pathways contribute to the structure of SS_{80}. A comparison of ^1H NMR spectra of the soluble fractions of SS_{80} and GS_{80} reveals similar general structural motifs (Figure 2 and Supplemental Figures S1 and S2), with resonances in SS_{80} appearing somewhat upfield versus the corresponding resonances in GS_{80} as expected due to the presence of an additional electron-releasing methoxy group on the syringol ring (Scheme 2).

The spectrum for SS_{80} reveals new resonances in the aromatic region (6.5–7.5 ppm) and in the methoxy group region (3.5–4 ppm) compared to parent syringol, confirming that the symmetry of the aryl ring has been broken, consistent with formation of S—C_{aryl} bonds. A broad resonance centered at 5.7 ppm was also observed in the spectrum of SS_{80}, attributable to a small fraction of aromatic rings undergoing dearomatization to give quinone derivatives 2g. Further structural insights were obtained by GC–MS analysis of the products of the reaction of syringol with elemental sulfur in various ratios as previously reported [104]. This analysis revealed that syringol underwent S—C_{aryl} bond formation to give both possible regioisomers of 2a and crosslinking of aryl rings via S—C_{aryl} bond formation as in compound 2b. In addition to S—C_{aryl} and S—C_{alkyl} bond formation, syringol has been observed to possess a remarkable capability to facilitate the formation of new C_{aryl}—C_{aryl} bonds with a thiol substituent in each aryl ring featuring two newly formed S—C_{aryl} bonds (2f) and O—C_{aryl} σ-bond scission of the methoxy group followed by S—C_{aryl} bond formation (2e). Thermal decomposition of syringol without sulfur leads to C—O σ-bond scission and loss of one or both methyl groups formed 2c-d species [104, 106, 107].

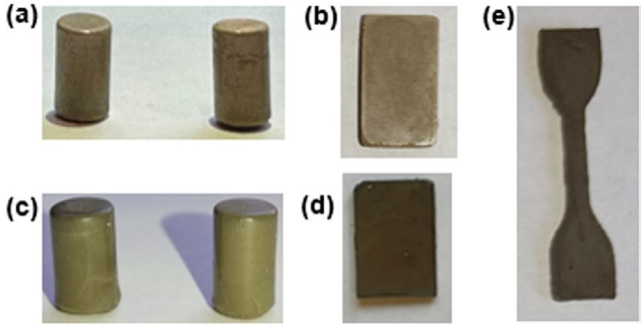

FIGURE 1 | Photos of (a) cylinders of GS_{80}, (b) rectangular prisms of GS_{80}, (c) cylinders of SS_{80}, (d) rectangular prisms of SS_{80}, and (e) a dog bone–shaped sample of SS_{80} for mechanical strength analysis.

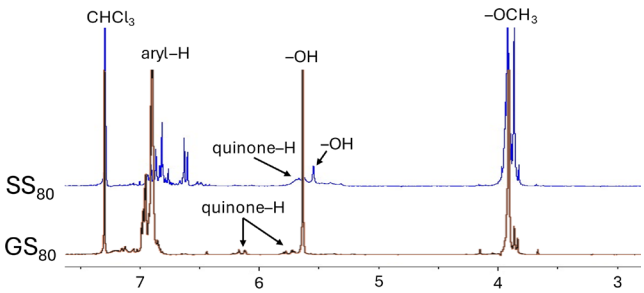

FIGURE 2 | Comparison of ^1H NMR spectra of the $CDCl_3$ soluble fractions of SS_{80} and GS_{80} highlighting the similar general structural motifs in both composites.

Since GS_{80} was originally reported, characteristics of HSMs have become more well-understood. Meticulous work by Hasell and coworkers, for example, has revealed that many HSMs contain not only polysulfide chains covalently anchored to organic comonomers (as shown in Scheme 1), but also other oligo and polysulfide chains and rings, collectively referred to as "dark sulfur" that are physically entrapped in the material [108, 109]. Because dark sulfur is not covalently anchored to the crosslinked network solid, it can be effectively extracted and quantified, either by mass balance or by a UV–vis method developed by Hasell et al., by spectroscopic analysis of dark sulfur extracted into ethyl acetate, a solvent in which the dark sulfur is selectively soluble. This analysis revealed dark sulfur-content percentages of 23 wt. % for GS_{80} and 53 wt. % for SS_{80}, respectively (Table 1).

2.2 | Thermal and Morphological Properties

Several methods were employed to assess the morphological and thermal behaviors of the composites. Scanning electron micrographs with element mapping by energy-dispersive X-ray analysis (EDX) of GS_{80} and SS_{80} showed a uniform sulfur, oxygen, and carbon distribution throughout both samples (Figure S7 in the SI).

Additional insight into the morphology of the composites was obtained from powder X-ray diffraction (PXRD, Figure S8 in the SI). PXRD reveals that both GS_{80} and SS_{80} exhibit amorphous character with a contribution of crystalline α-sulfur (orthorhombic sulfur). Differential scanning calorimetry (DSC) analysis was used to further quantify the percent crystallinity of the materials compared to that of α-sulfur, according to Equation (1), where ΔX_c is the change of percentage crystallinity with respect to sulfur, ΔH_m is the melting enthalpy of the composite, ΔH_{cc} is the cold crystallization enthalpy of the composite, $\Delta H_{m(S)}$ is the melting enthalpy of sulfur, and $\Delta H_{cc(S)}$ is the cold crystallization enthalpy of sulfur.

$$\Delta\chi_c = 1 - \left\{ \frac{\Delta H_m - \Delta H_{cc}}{\Delta H_{m(S)} - \Delta H_{cc(S)}} \right\} \times 100\,\% \quad (1)$$

The percent crystallinity of GS_{80} and SS_{80} was 8% and 38%, respectively, compared to pure elemental sulfur. Higher crystallinity in high sulfur materials correlates with increased dark sulfur content in the soluble fraction, indicating the relationship between polymer structure and sulfur distribution in these materials.

DSC analysis also showed characteristic endothermic phase transitions at 108°C and 105°C corresponding to phase change from the orthorhombic to the monoclinic allotrope of S_8 for GS_{80}

(A) General representation of SS_{80}

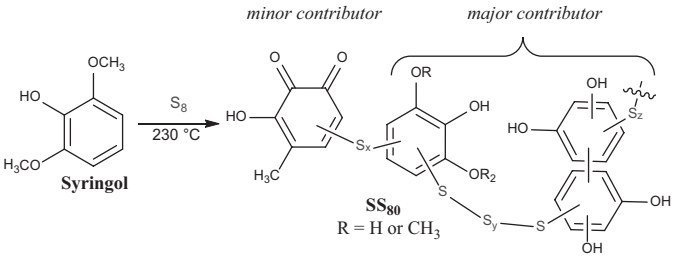

(B) Small molecules present in soluble fractions of SS_{80}

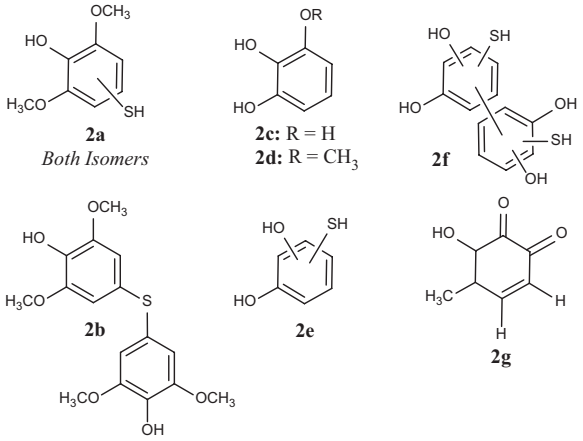

SCHEME 2 | The interaction between syringol and elemental sulfur leads to the formation of composite SS_{80} (A), an assignment assisted by analysis of soluble fractions (B).

TABLE 1 | Thermal and morphological properties of GS_{80} and SS_{80} compared to S_8.

Material	T_d[a]/°C	T_m[b]/°C	$T_{g,dsc}$[c]/°C	Percent crystallinity[d]	Dark sulfur (wt. %)[e]
GS_{80}	225	115	−34	8	23
SS_{80}	231	115	−36	36	53
S_8	229	118	NA	100	NA

[a]The onset temperature of the major mass loss by TGA.
[b]The temperature at the peak maximum of the endothermic melting.
[c]Glass transition temperature.
[d]The reduction of the percent crystallinity of each sample was calculated with respect to sulfur (normalized to 100%).
[e]Percent ethyl acetate-extractable sulfur species.

and SS_{80}, respectively. An endotherm at 115°C is attributed to the melting of monoclinic sulfur in sulfur-rich domains for both materials, while GS_{80} exhibited a $T_{g,\,DSC}$ of −34°C, similar to the value of −36°C for SS_{80}. These values are consistent with previously reported HSMs.

Thermogravimetric analysis (TGA) was used to determine the decomposition temperature of the products (T_d, here defined as the onset temperature of the major mass loss). Determination of the T_d in HSMs wherein both entrapped orthorhombic sulfur and crosslinked sulfur exist provides insight into the thermal stability of the materials and the contributions of the different components in the material. In GS_{80}, the first decomposition was observed at 94°C due to the loss of the remaining guaiacol. The major decompositions of GS_{80} and SS_{80} were observed at the 225°C and 231°C temperatures, respectively, due to the sublimation of entrapped cyclo-S_8. All the composites showed good thermal stability compared to the values observed from previously reported HSMs. A third decomposition was observed in GS_{80} at 322°C, attributable to the decomposition/volatilization of the organosulfur network of the material.

2.3 | Mechanical Properties

Insofar as mechanical properties, only tensile strength/elongation at break have been reported for GS_{80} previously [98]. For the current report, we determined those values for SS_{80} and expanded the range of mechanical metrics determined to include Shore hardness, flexural strength/modulus, compressional strength, and Young's modulus for both materials.

TABLE 2 | Comparison of mechanical properties of GS_{80} and SS_{80} composites to a range of chemically related HSMs, C62 Brick, and ordinary Portland cement.

Materials	Compressional strength (MPa)	Flexural strength/ modulus (MPa)	Ultimate tensile strength (MPa)	Young's modulus (MPa)	Elongation at break (%)	Shore (A) hardness
GS_{80}	5.2 ± 0.3	1.58 ± 0.02/8.4 ± 0.32	2.3 ± 0.02	14.5 ± 3.2	11 ± 2.1	85
SS_{80}	8.5 ± 0.5	2.16 ± 0.06/80 ± 31.6	3.8 ± 0.07	20.6 ± 3.8	10 ± 2.9	91
LS_{80}[a]	ND	2.1/87	ND	ND	ND	ND
CLS_{80}[b]	ND	> 3.6/248	ND	ND	ND	ND
XS_{81}[c]	ND	2.0/240	ND	ND	ND	ND
GS_{90}[d]	ND	ND	1.1 ± 0.53	47	4 ± 1.8	ND
GL_5S_{70}[e]	6.8 ± 0.1	2.3	ND	ND	ND	ND
GO_1S_{70}[f]	6.2 ± 0.1	1.9	ND	ND	ND	ND
ELS_{80}@180[g]	10.9	2.7	ND	ND	ND	ND
PGMA-S[h]	17.5 ± 2.8	4.8 ± 0.7/642	3.9 ± 1.20	11.1 ± 2.2	26 ± 8	ND
S-DCPD[i]	ND	6.0/3700	ND	ND	ND	ND
S-DCPD-linseed oil[j]	ND	4.7/1250	ND	ND	ND	ND
S-DCPD-limonene[k]	ND	1.9/1750	ND	ND	ND	ND
C62 Brick[l]	8.6	ND	ND	ND	ND	ND
Portland Cement	17.0	3.7/500	ND	ND	ND	ND

[a]Composite made by reaction of allyl lignin (20 wt. %) and sulfur (80 wt. %) [99].
[b]Composite made by reaction of chlorolignin (20 wt. %) and sulfur (80 wt. %) [86].
[c]Composite made by reaction of 2,4-dimethyl-3,5-dichlorophenol (DDP) (30 wt. %) and sulfur (70 wt. %) [36].
[d]Composite made by reaction of guaiacol (10 wt. %) and sulfur (90 wt. %) [98].
[e]Composite made by reaction of guaiacol (25 wt. %), linoleic acid (5 wt. %), and sulfur (70 wt. %) [103].
[f]Composite made by reaction of guaiacol (29 wt. %), oleic acid (1 wt. %), and sulfur (70 wt. %) [103].
[g]Composite made by reaction of esterified lignin (20 wt. %) and sulfur (80 wt. %) heated at 180°C [37].
[h]Composite made by reaction of olefin-derivatized (Geraniol) PMMA (10 wt. %) and sulfur (90 wt. %) [114].
[i]Composite made by reaction of dicyclopentadiene (DCPD) (50 wt. %) and sulfur (50 wt. %) [115].
[j]Composite made by reaction of DCPD (25 wt. %), linseed oil (25 wt. %), and sulfur (50 wt. %) [115].
[k]Composite made by reaction of DCPD (25 wt. %), limonene (25 wt. %), and sulfur (50 wt. %) [115].
[l]Brick classification C62 for building brick with negligible weathering.

Shore hardness measurements (Table 2) using a durometer revealed that SS_{80} (91 on the Shore A Scale) was slightly harder than GS_{80} (85 on the Shore A Scale). The Shore hardness (A) of both materials is in the range for organic rigid rubbers and synthetic resins, including polyurethane thermoplastic elastomers (70 A), ethylene vinyl acetate (85 A), and plasticized polyvinyl chloride (85 A) of the type used for familiar commercial items such as shoe heels, leather belts, skateboard wheels, and shopping cart wheels [110–113].

Cylindrical specimens (Figure 1) of GS_{80} and SS_{80} were used as test samples to determine their compressional strengths (Table 2; stress–strain plot provided in Figures S9, S10 in the SI). These tests revealed that GS_{80} and SS_{80} had compressional strength of 5.2 MPa and 8.5 MPa, respectively. The compressional strengths of GS_{80} and SS_{80} were similar to those of several previously reported HSMs derived from lignin derivatives (Table 2). For example, GL_5S_{70} (made from 25 wt. % guaiacol, 5 wt. % linoleic acid, and 70 wt. % sulfur) has a compressional strength of 6.8 MPa and GO_1S_{70} (made from 29 wt. % guaiacol, 1 wt. % linoleic acid, and 70 wt. % sulfur) had a compressional strength of 6.2 MPa [103]. In contrast, composite ELS_{80}@180 (prepared by the reaction of 20 wt. % oleyl-esterified lignin and 80 wt. % sulfur) had a higher compressional strength of 10.9 MPa, likely attributable to higher crosslinking afforded by whole lignin as compared to the small molecular lignin aromatics used to prepare GS_{80} and SS_{80} [37]. To put these values in perspective, familiar building materials like ordinary Portland cement (OPC) and C62 brick (general construction bricks) have compressional strengths of ≥ 17 MPa and 8.6 MPa, respectively.

Flexural strength analyses of rectangular prisms of GS_{80} and SS_{80} (Figure 1b,d) were conducted in single cantilever mode at room temperature (Table 2; stress–strain plot provided in Figures S11,S12 in the SI). These tests showed that GS_{80} and SS_{80} had a flexural strength of 1.58 MPa and 2.16 MPa, somewhat lower than that of OPC (3.7 MPa) but comparable to several other HSMs made from lignin or lignin derivatives (Table 2) [37, 86, 99, 103]. HSMs prepared from other organic components can exhibit notably higher flexural strengths. For example, S-DCPD (prepared from 50 wt. % dicyclopentadiene and 50 wt. % sulfur) has a higher flexural strength of 6.0 MPa. Replacing dicyclopentadiene with other organics was observed to lower the flexural strength, as illustrated by S-DCPD-linseed (50 wt. % sulfur, 25 wt. % DCPD, 25 wt. % linseed oil, and flexural strength = 4.7 MPa) and S-DCPD-limonene (50 wt. % sulfur, 25 wt. % DCPD, 25 wt. % limonene, and flexural strength = 1.9 MPa) [115]. These trends all reflect a general increase in flexural strength with increasing S–C crosslinking.

Tensile testing (Table 2) was undertaken to determine the ultimate tensile strength (UTS) at break, elongation at break, and Young's modulus for each composite using dog bone–shaped test specimens (Figure 1). SS_{80} had a higher UTS (3.85 MPa) than that of GS_{80} (2.16 MPa), and the compounds had similar elongations at break (9.93% for SS_{80} and 10.9%for GS_{80}). SS_{80} had an UTS equal within statistical limits to that of PGMA-S (a HSM prepared from 10 wt. % geranyl-derivatized PMMA and 90 wt. % sulfur and having an UTS = 3.88 MPa), but had a lower elongation at break (26%) than PGMA-S [114]. GS_{80} and SS_{80} showed greater elongation at break than the S-DCPD-linseed (1.3%) and S-DCPD-limonene terpolymer (5.5%), while S-DCPD was too brittle for tensile strength analysis [115]. GS_{80} and SS_{80} had elongation at break values comparable to or exceeding those of some commonly used polymers such as polystyrene (1.6%), epoxy resins (1.3%), phenol-formaldehyde (1.2%), and acrylonitrile–butadiene–styrene (6%), but significantly lower than those of others such as polyethylene terephthalate (300%), polycarbonate (200%), or polypropylene (80%) [112].

The Young's moduli for GS_{80} and SS_{80} were derived from the stress–strain plots for tensile strength analysis (Table 2; stress–strain plot provided in Figures S13, S14 in the SI). SS_{80} exhibited a value of 20.6 MPa compared to GS_{80} (14.5 MPa) and PGMA-S (11.1 MPa), indicating greater stiffness and resistance to deformation under applied stress. The Young's moduli for GS_{80} and SS_{80} lie within the range of commercial rubber formulations (10–100 MPa) but significantly lower values compared to many commodity plastics, including polypropylene (1500–2000 MPa), polyethylene terephthalate (2000–2700 MPa), polycarbonate (2600 MPa), and polystyrene (3000–3500 MPa) [113]. This limitation might impact the potential applications of composites.

3 | Conclusion

The development of SS_{80}, a lignin–sulfur composite synthesized from syringol and elemental sulfur, marks a significant advancement in the valorization of lignin by-products. Our study demonstrated that SS_{80}, formed by reacting 20 wt. % syringol with 80 wt. % sulfur, exhibits promising thermal and mechanical properties, positioning it as a potential sustainable material for various applications.

Thermogravimetric and DSC analyses revealed that SS_{80} has a higher crystallinity (38%) than does GS_{80} (8%) and exhibits greater thermal stability with a decomposition temperature of 231°C. This increased stability is attributable to the higher content of dark sulfur in SS_{80}. The presence of $S—C_{aryl}$ and $S—C_{alkyl}$ bonds, confirmed through GC–MS and ^1H NMR spectroscopy, highlights the robust chemical structure of SS_{80}.

Mechanical testing provided further insights into the material's capabilities. SS_{80} exhibited a compressional strength of 8.5 MPa, significantly higher than GS_{80} (5.2 MPa), and a flexural strength of 2.16 MPa compared to GS_{80} (1.58) MPa. These values are comparable to those of other HSMs and familiar conventional building materials such as C62 brick. Additionally, that SS_{80} had a Shore hardness of 91 and Young's modulus of 20.6 MPa indicate greater rigidity and resistance to deformation than GS_{80}, making it suitable for applications requiring durable and flexible materials.

The successful synthesis and characterization of SS_{80} underscores the potential of lignin-derived composites in advancing sustainable material science. By leveraging syringol's unique properties, SS_{80} offers a bio-based, high-performance alternative to traditional materials, addressing both lignin and sulfur waste challenges. Future research should explore the scalability of SS_{80} production and its performance in real-world applications, further cementing its role in sustainable material innovation.

4 | Experimental Section

4.1 | Chemicals and Materials

Syringol (99%) and sulfur powder (99.5%) were purchased from Sigma-Aldrich and Alfa Aesar, respectively. These chemicals were used without further purification. GS_{80} was prepared following the literature procedure [98].

4.2 | Instrumentation

Proton NMR spectra were acquired on a Bruker NEO-300 MHz (Bruker Biospin Corp., Billerica, MA, USA) at room temperature, and data were processed with SpinWorks 4.2.11 software.

The GC–MS analysis was carried out on a Shimadzu QP2010SE system with an auto-injector (AOC-20i) equipped with the mass selective detector, having an interface temperature of 250°C, a solvent cut time of 3.00 min, the threshold of 70 eV and mass range of 45–900 m/z. Compounds were separated using a SH-Rxi-5 MS capillary column (Restek Company, Bellefonte, USA: crossbond 5% diphenyl/95% dimethyl polysiloxane) having dimensions 30 m (length) × 0.25 mm (diameter) × 0.25 μm (film thickness). The temperature of the injector was initialized to 250°C. The temperature was programmed 50°C for 1 min, then from 50°C to 320°C at a rpm rate of 20°C/min, 320°C for 4 min.

TGA (Mettler Toledo, Columbus, OH, USA) data were recorded on a TA SDT Q600 instrument over the range 25°C–800°C, with a heating rate of 10°C·min^{-1} under a flow of N_2 (20 mL min^{-1}).

DSC data were acquired (Mettler Toledo DSC 3 STARe System, Mettler Toledo, Columbus, OH, USA) over the range −60°C to 140°C with a heating rate of 10°C min^{-1} under a flow of N_2 (200 mL min^{-1}). Each DSC measurement was carried out over three heat–cool cycles.

Compressional analysis was performed on a Mark-10 ES30 (Mark-10 Corporation Copiague, NY, USA) test stand with a M3-200 force gauge (1 kN maximum force with ±1 N resolution) by a modified ASTM C39 standard. Compression cylinders were cast from silicone resin molds (Smooth-On Oomoo 25 tin-cure, Oomoo Corp., Richmond, BC, Canada) with diameters of approximately 6 mm and heights of approximately 10 mm. Samples were manually sanded to ensure uniform dimensions and measured with a digital caliper with ±0.01 mm resolution. Analysis was performed in triplicate, and the reported results are an average of the runs.

Tensile measurements were taken with a Mark-10 ES30 (Mark-10 Corporation Copiague, NY, USA) mechanical test stand equipped with a Mark 1000 N Force Gauge (Model M3-200). The specimens were molded into dog bone shapes. A cross-section of the linear portion of the dog bones was used to calculate the specimen's stress. The thickness, width, and length were measured using a digital caliper (±0.01 mm resolution) in several sample areas. The average sample dimensions were 2.5 × 2.7 × 12.8 mm. Each sample was clamped with a Mark 10 wedge grip (Model G1061-1). Analysis was performed in triplicate, and the reported results are an average of the runs.

Flexural strength analysis was performed using a Mettler Toledo DMA 1 STARe System (Mettler Toledo, Columbus, OH, USA) in single cantilever mode. The samples were cast from silicone resin molds (Smooth-On Oomoo 25 tin-cure). The sample dimensions were approximately 1.5 × 10 × 18 mm. Sample dimensions were measured using a digital caliper with 0.01-mm resolution. The clamping force was 1 cN·m, and performing force was varied from 0 to 10 N with a ramp rate of 0.2 N·min^{-1} measured isothermally at 25°C. Analysis was performed in triplicate, and the reported results are an average of the runs.

PXRD was performed using a Rigaku SmartLab powder X-ray diffractometer (Rigaku is Tokyo, Japan), Cu Kα radiation (λ = 1.5406 Å) radiation, 2θ measuring range: 5°–80°, scan speed 10 min^{-1}, and step size 0.01°.

UV–vis data were collected on an Agilent Technologies Cary 60 UV–vis (Agilent Technologies Inc. Santa Clara, CA, USA) using Simple Reads software.

SEM and EDX were acquired on a Schottky Field Emission Scanning Electron Microscope SU5000 (Hitachi High-Tech, Tokyo, Japan) operating in variable pressure mode with an accelerating voltage of 15 keV.

Shore hardness was measured using a Shore A durometer (Gain Express Holdings Ltd., Kowloon, Hong Kong) with a range of 0–100 HA, resolution of 0.5 HA, total measure force of 8.1 N, and outside pressure of 1 kg. The measurements were performed according to ISO 7619 for rubber hardness determination. The thickness of the measured samples was 6 mm, and the values in three points were recorded. The average of the three values was taken as the sample's hardness.

4.3 | Synthesis of SS_{80}

CAUTION: Heating elemental sulfur with organics can result in the formation of H_2S or other gases. Such gases can be toxic, foul-smelling, and corrosive. Temperature must be carefully controlled to prevent thermal spikes, contributing to the potential for H_2S or other gas evolution. Rapid stirring shortened heating times, and very slow addition of reagents can help avoid unforeseen temperature spikes.

Elemental sulfur (72.00 g, 2245 mmol of S atom) and syringol (18.00 g, 116.8 mmol) were weighed directly into a glass pressure flask under a nitrogen atmosphere in a VTI glovebox. The flask was sealed with a PTFE screwcap equipped with a Viton O-ring. The flask was then placed in an oil bath, heated to a temperature of 230°C, and heated for 24 h with continuous stirring by a magnetic stir bar. After 24 h, the flask was cooled to room temperature, and a dark brown solid was collected for further analysis. This solid is termed SS_{80} in the manuscript.

Elemental analysis calculated: C, 12.46; S, 80.00; H, 1.31%. Found: C, 12.70; S, 79.20; H, 1.13%. (Atlantic Microlab Inc.).

4.4 | Determination of Dark Sulfur Content

A modified literature method for quantification of the dark sulfur content was employed by UV–vis spectroscopy in ethyl acetate to determine the dark sulfur content [108]. GS_{80} and SS_{80}, weighed with a microbalance between 6 and 7 mg, were added to 250-mL volumetric flasks with approximately 230 mL of ethyl acetate. The mixtures were allowed to stir for 30 min, after which the solutions were made up to the mark of 250 mL with ethyl acetate. A 3-mL aliquot of each solution was transferred to two separate cuvettes, and 3 mL of pure ethyl acetate was transferred to another cuvette to serve as a blank. Data were collected at 275 nm, and dark sulfur content was calculated from a calibration curve having the equation $y = 36.124x + 0.012$ ($R^2 = 0.9967$), where y is absorbance and x is the concentration of sulfur in mg/mL.

Acknowledgments

This research was funded by the National Science Foundation grant number CHE-2203669.

References

1. S. Bertella and J. S. Luterbacher, "Lignin Functionalization for the Production of Novel Materials," *Trends in Chemistry* 2 (2020): 440–453.

2. A. Tribot, G. Amer, M. Abdou Alio, et al., "Wood-Lignin: Supply, Extraction Processes and Use as Bio-Based Material," *European Polymer Journal* 112 (2019): 228–240.

3. M. S. Ganewatta, H. N. Lokupitiya, and C. Tang, "Lignin Biopolymers in the Age of Controlled Polymerization," *Polymers* 11 (2019): 1176.

4. D. S. Bajwa, G. Pourhashem, A. H. Ullah, and S. G. Bajwa, "A Concise Review of Current Lignin Production, Applications, Products and Their Environmental Impact," *Industrial Crops and Products* 139, no. 111 (2019): 526.

5. W. O. S. Doherty, P. Mousavioun, and C. M. Fellows, "Value-Adding to Cellulosic Ethanol: Lignin Polymers," *Industrial Crops and Products* 33 (2011): 259–276.

6. M. V. Rodionova, A. M. Bozieva, S. K. Zharmukhamedov, et al., "A Comprehensive Review on Lignocellulosic Biomass Biorefinery for Sustainable Biofuel Production," *International Journal of Hydrogen Energy* 47 (2022): 1481–1498.

7. R. Rinaldi, R. Jastrzebski, M. T. Clough, et al., "Paving the Way for Lignin Valorisation: Recent Advances in Bioengineering, Biorefining and Catalysis," *Angewandte Chemie (International Ed. in English)* 55 (2016): 8164–8215.

8. S. Banu Jamaldheen, M. B. Kurade, B. Basak, et al., "A Review on Physico-Chemical Delignification as a Pretreatment of Lignocellulosic Biomass for Enhanced Bioconversion," *Bioresource Technology* 346, no. 126 (2022): 591.

9. M. V. Tsvetkov and E. A. Salganskii, "Lignin: Applications and Ways of Utilization (Review)," *Russian Journal of Applied Chemistry* 91 (2018): 1129–1136.

10. K. Wang, K. H. Kim, and R. C. Brown, "Catalytic Pyrolysis of Individual Components of Lignocellulosic Biomass," *Green Chemistry* 16 (2014): 727–735.

11. Z. Sun, J. Cheng, D. Wang, T.-Q. Yuan, G. Song, and K. Barta, "Downstream Processing Strategies for Lignin-First Biorefinery," *ChemSusChem* 13 (2020): 5199–5212.

12. Z. Sun, B. Fridrich, A. de Santi, S. Elangovan, and K. Barta, "Bright Side of Lignin Depolymerization: Toward New Platform Chemicals," *Chemical Reviews* 118 (2018): 614–678.

13. M. V. Galkin and J. S. M. Samec, "Lignin Valorization through Catalytic Lignocellulose Fractionation: A Fundamental Platform for the Future Biorefinery," *ChemSusChem* 9 (2016): 1544–1558.

14. M. A. Taher, X. Wang, K. M. Faridul Hasan, M. R. Miah, J. Zhu, and J. Chen, "Lignin Modification for Enhanced Performance of Polymer Composites," *ACS Applied Bio Materials* 6 (2023): 5169–5192.

15. S. S. Wong, R. Shu, J. Zhang, H. Liu, and N. Yan, "Downstream Processing of Lignin Derived Feedstock into End Products," *Chemical Society Reviews* 49 (2020): 5510–5560.

16. D. Esposito and M. Antonietti, "Redefining Biorefinery: The Search for Unconventional Building Blocks for Materials," *Chemical Society Reviews* 44 (2015): 5821–5835.

17. X. Bai, K. H. Kim, R. C. Brown, et al., "Formation of Phenolic Oligomers During Fast Pyrolysis of Lignin," *Fuel* 128 (2014): 170–179.

18. L. Jiang, C.-G. Wang, P. L. Chee, et al., "Strategies for Lignin Depolymerization and Reconstruction Towards Functional Polymers," *Sustainable Energy & Fuels* 7 (2023): 2953–2973.

19. S. L. Kristufek, K. T. Wacker, Y.-Y. T. Tsao, L. Su, and K. L. Wooley, "Monomer Design Strategies to Create Natural Product-Based Polymer Materials," *Natural Product Reports* 34 (2017): 433–459.

20. G. F. Bass and T. H. Epps, "Recent Developments Towards Performance-Enhancing Lignin-Based Polymers," *Polymer Chemistry* 12 (2021): 4130–4158.

21. X. Lu and X. Gu, "A Review on Lignin-Based Epoxy Resins: Lignin Effects on Their Synthesis and Properties," *International Journal of Biological Macromolecules* 229 (2023): 778–790.

22. Y. Yang, Y. Wang, M. Zhu, J. Zhao, D. Cai, and H. Cao, "Valorization of Lignin for Renewable Non-Isocyanate Polyurethanes: A State-of-the-Art Review," *Materials Today Sustainability* 22, no. 22 (2023): 100367.

23. A. H. Iswanto, M. A. R. Lubis, J. Sutiawan, et al., "Latest Advancements in the Development of High-Performance Lignin- and Tannin-Based Non-Isocyanate Polyurethane Adhesive for Wood Composites," *Polymers (Basel, Switzerland)* 15 (2023): 3864.

24. S. V. Mhatre, J. S. Mahajan, T. H. Epps, and L. T. J. Korley, "Lignin-Derivable Alternatives to Petroleum-Derived Non-Isocyanate Polyurethane Thermosets With Enhanced Toughness," *Materials Advances* 4 (2023): 110–121.

25. T. R. Araujo, D. Bresolin, D. de Oliveira, C. Sayer, P. H. H. de Araujo, and J. V. de Oliveira, "Conventional Lignin Functionalization for Polyurethane Applications and a Future Vision in the Use of Enzymes as an Alternative Method," *European Polymer Journal* 188 (2023): 111934.

26. S.-L. Zou, L.-P. Xiao, W.-Z. Yin, et al., "Biodegradable, Recyclable, Waterproof, Antibacterial and High-Strength Supramolecular Plastic Fabricated From Lignin Derivatives," *Sustainable Materials and Technologies* 39 (2024): e00861.

27. R. M. O'Dea, P. A. Pranda, Y. Luo, et al., "Ambient-Pressure Lignin Valorization to High-Performance Polymers by Intensified Reductive Catalytic Deconstruction," *Science Advances* 8 (2022): eabj7523.

28. M. A. Salami, F. Kaveian, M. Rafienia, S. Saber-Samandari, A. Khandan, and M. Naeimi, "Electrospun Polycaprolactone/lignin-based Nanocomposite as a Novel Tissue Scaffold for Biomedical Applications," *Journal of Medical Signals and Sensors* 7 (2017): 228–238.

29. US Geological Survey, "Sulfur Production Worldwide in 2022, By Country," https://www-statista-com.libproxy.clemson.edu/statistics/1031181/sulfur-production-globally-by-country/, (2023).

30. N. Gupta, P. K. Roychoudhury, and J. K. Deb, "Biotechnology of Desulfurization of Diesel: Prospects and Challenges," *Applied Microbiology and Biotechnology* 66 (2005): 356–366.

31. A. Tanimu and K. Alhooshani, "Advanced Hydrodesulfurization Catalysts: A Review of Design and Synthesis," *Energy & Fuels* 33 (2019): 2810–2838.

32. P. Yan, W. Zhao, S. J. Tonkin, J. M. Chalker, T. L. Schiller, and T. Hasell, "Stretchable and Durable Inverse Vulcanized Polymers with Chemical and Thermal Recycling," *Chemistry of Materials* 34 (2022): 1167–1178.

33. P. D. McNaughter, P. O'Brien, J. C. Bear, I. P. Parkin, A. G. Mayes, and P. O'Brien, "Thein Situsynthesis of PbS Nanocrystals From Lead(II) n-Octylxanthate Within a 1,3-Diisopropenylbenzene–Bisphenol a Dimethacrylate Sulfur Copolymer," *Royal Society Open Science* 4, no. 8 (2017): 170383.

34. K.-S. Kang, C. Olikagu, T. Lee, et al., "Sulfenyl Chlorides: An Alternative Monomer Feedstock from Elemental Sulfur for Polymer Synthesis," *Journal of the American Chemical Society* 144, no. 23 (2022): 23044–23052.

35. A. Hoefling, D. T. Nguyen, Y. J. Lee, S.-W. Song, and P. Theato, "A Sulfur–Eugenol Allyl Ether Copolymer: A Material Synthesized via Inverse Vulcanization From Renewable Resources and its Application in Li–S Batteries," *Materials Chemistry Frontiers* 1 (2017): 1.

36. M. S. Karunarathna, M. K. Lauer, A. G. Tennyson, and R. C. Smith, "Copolymerization of an Aryl Halide and Elemental Sulfur as a Route to High Sulfur Content Materials," *Polymer Chemistry* 11 (2020): 1621–1628.

37. M. S. Karunarathna, C. P. Maladeniya, M. K. Lauer, A. G. Tennyson, and R. C. Smith, "Durable Composites by Vulcanization of Oleyl-Esterified Lignin," *RSC Advances* 13 (2023): 3234–3240.

38. O. Bayram, B. Kiskan, E. Demir, R. Demir-Cakan, and Y. Yagci, "Advanced Thermosets from Sulfur and Renewable Benzoxazine and Ionones via Inverse Vulcanization," *ACS Sustainable Chemistry & Engineering* 8 (2020): 9145–9155.

39. A. E. Davis, K. B. Sayer, and C. L. Jenkins, "A comparison of Adhesive Polysulfides Initiated by Garlic Essential Oil and Elemental Sulfur to Create Recyclable Adhesives," *Polymer Chemistry* 13 (2022): 4634–4640.

40. C. Herrera, K. J. Ysinga, and C. L. Jenkins, "Polysulfides Synthesized from Renewable Garlic Components and Repurposed Sulfur Form Environmentally Friendly Adhesives," *ACS Applied Materials & Interfaces* 11, no. 35 (2019): 35312–35318.

41. A. D. Tikoalu, N. A. Lundquist, and J. M. Chalker, "Mercury Sorbents Made By Inverse Vulcanization of Sustainable Triglycerides: The Plant Oil Structure Influences the Rate of Mercury Removal from Water," *Advanced Sustainable Systems* 4 (2020): 1900111.

42. C. V. Lopez, A. D. Smith, and R. C. Smith, "High Strength Composites From Low-Value Animal Coproducts and Industrial Waste Sulfur," *RSC Advances* 12 (2022): 1535–1542.

43. M. K. Lauer, A. G. Tennyson, and R. C. Smith, "Green Synthesis of Thermoplastic Composites from a Terpenoid-Cellulose Ester," *ACS Applied Polymer Materials* 2 (2020): 3761–3765.

44. A. D. Smith, A. G. Tennyson, and R. C. Smith, "Sulfur-Containing Polymers Prepared From Fatty Acid-Derived Monomers: Application of Atom-Economical Thiol-Ene/Thiol-Yne Click Reactions and Inverse Vulcanization Strategies," *Sustainable Chemistry* 1 (2020): 209–237.

45. F. Stojcevski, M. K. Stanfield, D. J. Hayne, et al., "Inverse Vulcanisation of Canola Oil as a Route to Recyclable Chopped Carbon Fibre Composites," *Sustainable Materials and Technologies* 32 (2022): e00400.

46. A. Gupta, M. J. H. Worthington, H. D. Patel, M. R. Johnston, M. Puri, and J. M. Chalker, "Reaction of Sulfur and Sustainable Algae Oil for Polymer Synthesis and Enrichment of Saturated Triglycerides," *ACS Sustainable Chemistry & Engineering* 10 (2022): 9022–9028.

47. X. Wang, J. Qiao, Z. Zhou, et al., "Elastomeric Nanoparticles: Effective AdditiveFor High Performance Rubber Nanocomposites," *Rubber Chemistry and Technology* 93 (2020): 445–456.

48. A. Abbasi, M. M. Nasef, and W. Z. N. Yahya, "Copolymerization of Vegetable Oils and Bio-Based Monomers With Elemental Sulfur: A New Promising Route for Bio-Based Polymers," *Sustainable Chemistry and Pharmacy* 13, no. 100 (2019): 158.

49. C. P. Maladeniya, M. S. Karunarathna, M. K. Lauer, C. V. Lopez, T. Thiounn, and R. C. Smith, "A Role for Terpenoid Cyclization in the Atom Economical Polymerization of Terpenoids With Sulfur to Yield Durable Composites," *Materials Advances* 1 (2020): 1665–1674.

50. Y. Ren, K. Xu, J. Peng, Y. Xing, S. Gao, and M. Chen, "Preparation and Thermostability of Terpenes/Sulfur Oligomer," *Huagong Xuebao (Chinese Edition)* 67 (2016): 1580.

51. M. Firdaus, L. Montero de Espinosa, and M. A. R. Meier, "Terpene-Based Renewable Monomers and Polymers via Thiol–Ene Additions," in *Macromolecules*, vol. 44 (Washington, DC, United States: American Chemical Society, 2011), 7253–7262.

52. J. J. Griebel, S. Namnabat, E. T. Kim, et al., "New Infrared Transmitting Material via Inverse Vulcanization of Elemental Sulfur to Prepare High Refractive Index Polymers," in *Advanced Materials*, vol. 26 (Weinheim, Germany: John Wiley and Sons, 2014), 3014–3018.

53. J. J. Griebel, N. A. Nguyen, S. Namnabat, et al., "Dynamic Covalent Polymers via Inverse Vulcanization of Elemental Sulfur for Healable Infrared Optical Materials," *ACS Macro Letters* 4 (2015): 862–866.

54. S. Namnabat, J. J. Gabriel, J. Pyun, R. A. Norwood, E. L. Dereniak, and J. van der Laan, "Document Details—Optical Properties of Sulfur Copolymers for Infrared Applications," *Proceedings of SPIE* 8983 (2014): 89830.

55. T. S. Kleine, R. S. Glass, D. L. Lichtenberger, et al., "100th Anniversary of Macromolecular Science Viewpoint: High Refractive Index Polymers from Elemental Sulfur for Infrared Thermal Imaging and Optics," *ACS Macro Letters* 9 (2020): 245–259.

56. S. Park, D. Lee, H. Cho, J. Lim, and K. Char, "Inverse Vulcanization Polymers with Enhanced Thermal Properties via Divinylbenzene Homopolymerization-Assisted Cross-Linking," *ACS Macro Letters* 8 (2019): 1670–1675.

57. J. J. Griebel, G. Li, R. S. Glass, K. Char, and J. Pyun, "Kilogram Scale Inverse Vulcanization of Elemental Sulfur to Prepare High Capacity Polymer Electrodes for Li-S Batteries," *Journal of Polymer Science Part A: Polymer Chemistry* 53 (2015): 173–177.

58. C. V. Lopez, C. P. Maladeniya, and R. C. Smith, "Lithium-Sulfur Batteries: Advances and Trends," *Electrochemistry* 1 (2020): 226–259.

59. Z. Chen, J. Droste, G. Zhai, et al., "Sulfur-Anchored Azulene as a Cathode Material for Li–S Batteries," *Chemical Communications* 55 (2019): 9047–9050.

60. P. T. Dirlam, A. G. Simmonds, T. S. Kleine, et al., "Inverse Vulcanization of Elemental Sulfur With 1,4-Diphenylbutadiyne for Cathode Materials in Li–S Batteries," *RSC Advances* 5, no. 24 (2015): 24718–24722.

61. W. J. Chung, J. J. Griebel, E. T. Kim, et al., "The Use of Elemental Sulfur as an Alternative Feedstock for Polymeric Materials," *Nature Chemistry* 5 (2013): 518–524.

62. I. Gomez, D. Mecerreyes, J. A. Blazquez, et al., "Inverse Vulcanization of Sulfur With Divinylbenzene: Stable and Easy Processable Cathode

Material for Lithium-Sulfur Batteries," *Journal of Power Sources* 329 (2016): 72–78.

63. I. Gomez, O. Leonet, J. A. Blazquez, and D. Mecerreyes, "Inverse Vulcanization of Sulfur using Natural Dienes as Sustainable Materials for Lithium–Sulfur Batteries," *ChemSusChem* 9 (2016): 3419–3425.

64. M. Arslan, B. Kiskan, E. C. Cengiz, R. Demir-Cakan, and Y. Yagci, "Inverse Vulcanization of Bismaleimide and Divinylbenzene by Elemental Sulfur for Lithium Sulfur Batteries," *European Polymer Journal* 80 (2016): 70–77.

65. H. Kang, H. Kim, and M. J. Park, "Sulfur-Rich Polymers with Functional Linkers for High-Capacity and Fast-Charging Lithium–Sulfur Batteries," *Advanced Energy Materials* 8 (2018): 1802423.

66. A. Ghosh, S. Shukla, G. S. Khosla, B. Lochab, and S. Mitra, "Sustainable Sulfur-rich Copolymer/Graphene Composite as Lithium-Sulfur Battery Cathode with Excellent Electrochemical Performance," *Scientific Reports* 6, no. 25 (2016): 25207.

67. S. F. do Valle, A. S. Giroto, H. P. G. Reis, G. G. F. Guimarães, and C. Ribeiro, "Synergy of Phosphate-Controlled Release and Sulfur Oxidation in Novel Polysulfide Composites for Sustainable Fertilization," *Journal of Agricultural and Food Chemistry* 69 (2021): 2392–2402.

68. S. F. Valle, A. S. Giroto, R. Klaic, G. G. F. Guimaraes, and C. Ribeiro, "Sulfur Fertilizer Based on Inverse Vulcanization Process With Soybean Oil," *Polymer Degradation and Stability* 162 (2019): 102–105.

69. M. Mann, J. E. Kruger, F. Andari, et al., "Sulfur Polymer Composites as Controlled-Release Fertilisers," *Organic & Biomolecular Chemistry* 17 (2018): 1929–1936.

70. Y. Fu, C. Yang, Y. Zheng, et al., "Sulfur Crosslinked Poly(m-Aminothiophenol)/Potato Starch on Mesoporous Silica for Efficient Hg(II) Removal and Reutilization of Waste Adsorbent as a Catalyst," *Journal of Molecular Liquids* 328, no. 115 (2021): 115420.

71. H.-K. Lin, Y.-S. Lai, and Y.-L. Liu, "Cross-Linkable and Self-Foaming Polysulfide Materials for Repairable and Mercury Capture Applications," *ACS Sustainable Chemistry & Engineering* 7 (2019): 4515–4522.

72. M. W. Thielke, L. A. Bultema, D. D. Brauer, P. Theato, B. Richter, and M. Fischer, "Rapid Mercury(II) Removal by Electrospun Sulfur Copolymers," *Polymers (Basel)* 8 (2016): 266.

73. M. L. Eder, C. B. Call, and C. L. Jenkins, "Utilizing Reclaimed Petroleum Waste to Synthesize Water-Soluble Polysulfides for Selective Heavy Metal Binding and Detection," *ACS Applied Polymer Materials* 4 (2022): 1110–1116.

74. T. Hasell, D. J. Parker, H. A. Jones, T. McAllister, and S. M. Howdle, "Porous Inverse Vulcanised Polymers for Mercury Capture," *Chemical Communications* 52 (2016): 5383–5386.

75. M. P. Crockett, A. M. Evans, M. J. H. Worthington, et al., "Sulfur-Limonene Polysulfide: A Material Synthesized Entirely From Industrial By-Products and its Use in Removing Toxic Metals From Water and Soil," *Angewandte Chemie, International Edition* 55 (2016): 1714–1718.

76. M. J. H. Worthington, R. L. Kucera, I. S. Albuquerque, et al., "Laying Waste to Mercury: Inexpensive Sorbents Made from Sulfur and Recycled Cooking Oils," *Chemistry—A European Journal* 23, no. 16 (2017): 16219–16230.

77. D. J. Parker, H. A. Jones, S. Petcher, et al., "Low Cost and Renewable Sulfur-Polymers by Inverse Vulcanisation, and Their Potential for Mercury Capture," *Journal of Materials Chemistry A: Materials for Energy and Sustainability* 5, no. 11 (2017): 11682–11692.

78. J.-S. M. Lee, D. J. Parker, A. I. Cooper, and T. Hasell, "High Surface Area Sulfur-Doped Microporous Carbons from Inverse Vulcanised Polymers," *Journal of Materials Chemistry A: Materials for Energy and Sustainability* 5, no. 18 (2017): 18603–18605.

79. S. Petcher, D. J. Parker, and T. Hasell, "Macroporous Sulfur Polymers From a Sodium Chloride Porogen—A Low Cost, Versatile Remediation Material," *Environmental Science: Water Research & Technology* 5 (2019): 2142–2149.

80. J. M. Scheiger, C. Direksilp, P. Falkenstein, et al., "Inverse Vulcanization of Styrylethyltrimethoxysilane–Coated Surfaces, Particles, and Crosslinked Materials," *Angewandte Chemie, International Edition* 59, no. 18 (2020): 18639–18645.

81. J. M. Chalker, M. Mann, M. J. H. Worthington, and L. J. Esdaile, "Polymers Made by Inverse Vulcanization for Use as Mercury Sorbents," *Organic Materials* 3 (2021): 362–373.

82. F. G. Mueller, L. S. Lisboa, and J. M. Chalker, "Inverse Vulcanized Polymers for Sustainable Metal Remediation," *Advanced Sustainable Systems* 7 (2023): 2300010.

83. S. J. Tonkin, C. T. Gibson, J. A. Campbell, et al., "Chemically Induced Repair, Adhesion, and Recycling of Polymers Made by Inverse Vulcanization," *Chemical Science* 11 (2020): 5537–5546.

84. K. B. Sayer, V. L. Miller, Z. Merrill, A. E. Davis, and C. L. Jenkins, "Allyl Sulfides in Garlic Oil Initiate the Formation of Renewable Adhesives," *Polymer Chemistry* 14 (2023): 3091–3098.

85. M. E. Duarte, B. Huber, P. Theato, and H. Mutlu, "The Unrevealed Potential of Elemental Sulfur for the Synthesis of High Sulfur Content Bio-Based Aliphatic Polyesters," *Polymer Chemistry* 11 (2020): 241–248.

86. M. S. Karunarathna, A. G. Tennyson, and R. C. Smith, "Facile New Approach to High Sulfur-Content Materials and Preparation of Sulfur–Lignin Copolymers," *Journal of Materials Chemistry A* 8 (2020): 548–553.

87. M. K. Lauer, A. G. Tennyson, and R. C. Smith, "Inverse Vulcanization of Octenyl Succinate-Modified Corn Starch as a Route to Biopolymer–Sulfur Composites," *Materials Advances* 2 (2021): 2391–2397.

88. H.-K. Lin and Y.-L. Liu, "Sulfur Radical Transfer and Coupling Reaction to Benzoxazine Groups: A New Reaction Route for Preparation of Polymeric Materials Using Elemental Sulfur as a Feedstock," *Macromolecular Rapid Communications* 39 (2018): 1700832.

89. Y. Liu, Y. Chen, Y. Zhang, et al., "Density-Adjustable Bio-Based Polysulfide Composite Prepared by Inverse Vulcanization and Bio-Based Fillers," *Polymers* 12 (2020): 2127.

90. M. J. H. Worthington, R. L. Kucera, and J. M. Chalker, "Green Chemistry and Polymers Made From Sulfur," *Green Chemistry* 19 (2017): 2748–2761.

91. Y. Xin, H. Peng, J. Xu, and J. Zhang, "Ultrauniform Embedded Liquid Metal in Sulfur Polymers for Recyclable, Conductive, and Self-Healable Materials," *Advanced Functional Materials* 29 (2019): 1808989.

92. D. Wang, Z. Tang, S. Fang, et al., "The Use of Inverse Vulcanised Polysulfide as an Intelligent Interfacial Modifier in Rubber/Carbon Black Composites," *Carbon* 184 (2021): 409–417.

93. L. Sun, S. Gao, X. Gui, L. Liu, K. Xu, and H. Liu, "Renewable Sulfur- and Monoterpenes-Derived Polysulfides as Functional Crosslinker for Epoxy Thermosets," *European Polymer Journal* 123, no. 109 (2020): 109440.

94. J. Lim, J. Pyun, and K. Char, "Recent Approaches for the Direct Use of Elemental Sulfur in the Synthesis and Processing of Advanced Materials," *Angewandte Chemie, International Edition* 54 (2015): 3249–3258.

95. D. A. Boyd, "Sulfur and its Role in Modern Materials Science," *Angewandte Chemie, International Edition* 55, no. 15 (2016): 15486–15502.

96. S. Gwon, S.-Y. Oh, and M. Shin, "Strength and Microstructural Characteristics of Sulfur Polymer Composites Containing Binary Cement and Waste Rubber," *Construction and Building Materials* 181 (2018): 276–286.

97. C. Wongsirathat and O. Chavalparit, "Utilization of Sulfur Waste from Petroleum Refinery for Sulfur Concrete," in *Advanced Materials Research*, vol. 856 (Durnten-Zurich, Switzerland: Trans Tech Publications Ltd, 2014), 113–117.

98. M. S. Karunarathna, M. K. Lauer, and R. C. Smith, "Facile Route to an Organosulfur Composite From Biomass-Derived Guaiacol and Waste Sulfur," *Journal of Materials Chemistry A* 8, no. 20 (2020): 318.

99. M. S. Karunarathna, M. K. Lauer, T. Thiounn, R. C. Smith, and A. G. Tennyson, "Valorisation of Waste to Yield Recyclable Composites of Elemental Sulfur and Lignin," *Journal of Materials Chemistry A* 7, no. 15 (2019): 15683–15690.

100. N. L. Kapuge Dona, C. P. Maladeniya, and R. C. Smith, "Reactivity of Biomass-Derived Olefins with Elemental Sulfur: Mechanistic Insight," *European Journal of Organic Chemistry* 27 (2024): e202301269.

101. M. K. Lauer, M. S. Karunarathna, A. G. Tennyson, and R. C. Smith, "Robust, Remeltable and Remarkably Simple to Prepare Biomass–Sulfur Composites," *Materials Advances* 1 (2020): 2271–2278.

102. M. K. Lauer, M. S. Karunarathna, A. G. Tennyson, and R. C. Smith, "Recyclable, Sustainable, and stronger Than Portland Cement: A Composite From Unseparated Biomass and Fossil Fuel Waste," *Materials Advances* 1 (2020): 590–594.

103. C. P. Maladeniya, N. L. Kapuge Dona, A. D. Smith, and R. C. Smith, "Thermal and Mechanical Properties of Guaiacol–Fatty Acid-Sulfur Composites," *Macromolecules* 3 (2023): 681–692.

104. K. A. Tisdale, N. L. K. Dona, C. P. Maladeniya, and R. C. Smith, "Green and Atom Economical Route to High Compressive Strength Lignin Oil-Sulfur Composites," *Journal of Polymers and the Environment* 32, no. 10 (2024): 4842–4854.

105. D. Aebisher, M. Brzostowska Edyta, A. Mahendran, and A. Greer, "Regioselective (Biomimetic) Synthesis of a Pentasulfane From Ortho-Benzoquinone," *Journal of Organic Chemistry* 72 (2007): 2951–2955.

106. L. Li, R. Van de Vijver, and K. M. Van Geem, "Experimental and Kinetic Study on the Gas-Phase Pyrolysis of Syringol," *Energy & Fuels* 37 (2023): 7246–7259.

107. M. Asmadi, H. Kawamoto, and S. Saka, "Thermal Reactions of Guaiacol and Syringol as Lignin Model Aromatic Nuclei," *Journal of Analytical and Applied Pyrolysis* 92 (2011): 88–98.

108. J. J. Dale, J. Stanley, R. A. Dop, et al., "Exploring Inverse Vulcanisation Mechanisms From the Perspective of Dark Sulfur," *European Polymer Journal* 195, no. 112 (2023): 112198.

109. J. J. Dale, S. Petcher, and T. Hasell, "Dark Sulfur: Quantifying Unpolymerized Sulfur in Inverse Vulcanized Polymers," *ACS Applied Polymer Materials* 4 (2022): 3169–3173.

110. Q. Tang, J. He, R. Yang, and Q. Ai, "Study of the Synthesis and Bonding Properties of Reactive Hot-Melt Polyurethane Adhesive," *Journal of Applied Polymer Science* 128 (2013): 2152–2161.

111. "Shore A Hardness Scale: Definition, Uses, Types, Benefits, and Limitations," accessed March 30, 2024, https://www.xometry.com/resources/materials/shore-a-hardness-scale.

112. T. R. Crompton, *Physical Testing of Plastics* (Shropshire, UK: Smithers Rapra, 2012).

113. "Young's Modulus, Tensile Strength and Yield Strength Values for some Materials," accessed March 30, 2024, https://www.endangeredlanguages.com/lang/5342.

114. S. K. Wijeyatunga, K. M. Derr, C. P. Maladeniya, P. Y. Sauceda-Oloño, A. G. Tennyson, and R. C. Smith, "Upcycling Waste PMMA to Durable Composites via a Transesterification-Inverse Vulcanization Process," *Journal of Polymer Science* 62 (2024): 554–563.

115. T. Hasell, J. Smith, S. Green, et al., "Crosslinker Copolymerization for Property Control in Inverse Vulcanization," *Chemistry—A European Journal* (2019): 25.

Supporting Information

Additional supporting information can be found online in the Supporting Information section.